Journal of Hazardous Materials 403 (2021) 123597

Contents lists available at ScienceDirect

Journal of Hazardous Materials

journal homepage: www.elsevier.com/locate/jhazmat

A new DGT technique comprising a hybrid sensor for the simultaneous high resolution 2-D imaging of sulfides, metallic cations, oxyanions and dissolved oxygen

Mingyi Ren [a,b], Shiming Ding [a,c,*], Zhihui Dai [d,*], Jingfu Wang [e], Cai Li [f], Zhilin Zhong [a,b], Jingxin Cao [a,b], Liyuan Yang [f], Daniel C.W. Tsang [g], Shiwei Xu [h], Chenye Yang [h], Yan Wang [a,c]

[a] State Key Laboratory of Lake Science and Environment, Nanjing Institute of Geography and Limnology, Chinese Academy of Sciences, Nanjing 210008, China
[b] University of Chinese Academy of Sciences, Beijing 100049, China
[c] Nanjing EasySensor Environmental Technology Co., Ltd, Nanjing 210018, China
[d] State Key Laboratory of Ore Deposit Geochemistry, Institute of Geochemistry, Chinese Academy of Sciences, Guiyang 550081, China
[e] State Key Laboratory of Environmental Geochemistry, Institute of Geochemistry, Chinese Academy of Sciences, Guiyang 550081, China
[f] School of Resources and Environment, University of Jinan, Jinan 250022, China
[g] Department of Civil and Environmental Engineering, The Hong Kong Polytechnic University, Hung Hom, Kowloon, Hong Kong China
[h] Central Laboratory, Jiangsu Academy of Agricultural Science, Nanjing 210008, China

ARTICLE INFO

Editor: D. Aga

Keywords:
Oxyanion
Potentially toxic elements
Sulfide
Diffusive gradients in thin films
Planar optrode

ABSTRACT

A new diffusive gradients in thin films technique (HR-ZCA DGT) was developed for simultaneous two-dimensional (2-D) chemical imaging of sulfides, metallic cations and oxyanions (S, Cd, Co, Fe, Cu, Mn, Ni, Pb, Zn, As, Cr, Mo, Sb, Se, V, P and W) at the submillimeter scale, combined with laser ablation inductively coupled plasma mass spectrometry (LA-ICP-MS) analysis. A novel binding gel was prepared using a double precipitation method with AgI and zirconium oxide (Zr-oxide) deposited sequentially on a preformed Chelex-100 resin gel. A good linear relationship was observed (R^2>0.99) between mass accumulation of the 17 assessed elements on the binding gel and the corresponding standardized laser ablation signals (signals of elements divided by signals of internal standard ^{13}C), proving the feasibility of LA-ICP-MS analysis. Good analytical precision (RSD<12 %) was achieved for all 17 elements. A hybrid sensor comprising the novel DGT binding gel overlying an O_2 planar optrode was then tested in sediments to evaluate the dynamics of O_2 and multiple elements. Results showed that the mobility of As, P and W were controlled by precipitation/dissolution processes with Fe/Mn oxides. V, Co, Ni, Zn, Mo, Cd and Sb were released at the sediment surface with the oxidation of iron sulfides.

1. Introduction

Metallic cations (Cd, Co, Cu, Ni, Pb and Zn) and oxyanions (As, Cr, Mo, Sb, Se, V and W) are commonly detectable in the natural environment (Mishra et al., 2019; Sarwar et al., 2017; Weidner and Ciesielczyk, 2019). Among them, Cu, Zn, Mo, Co, V and Se are essential nutrients for animal and human (Zoroddu et al., 2019). Others are used as industrial materials (Khademi et al., 2019). Phosphorus (P) is an essential element, while also being a key factor contributing to eutrophication in aquatic environments (Schindler et al., 2016). In the natural environment, mobility and cycling of these elements are controlled by precipitation/dissolution processes which have a close relationship with the behavior of manganese (Mn), iron (Fe) and sulfur (S) (Amrane and Bouhidel, 2019; McKenzie, 1980; Ratié et al., 2019). In particular, dissolved sulfide has been shown to be the most important factor controlling trace metal distribution in anoxic sediments (Di Toro et al., 1990; Gao et al., 2015). In addition, direct or indirect interactions between multiple elements affect their behavior in the environment. Accordingly, simultaneous measurement of multiple elements is important to help understand biogeochemical cycles in the natural environment.

To avoid undesirable or unavoidable transformation during sampling, transportation and sample handling, diffusive gradients in thin films technique (DGT) (Davison and Zhang, 1994) has been used to

* Corresponding author at: State Key Laboratory of Lake Science and Environment, Nanjing Institute of Geography and Limnology, Chinese Academy of Sciences, Nanjing 210008, China.
E-mail addresses: smding@niglas.ac.cn (S. Ding), daizhihui@mails.gyig.ac.cn (Z. Dai).

https://doi.org/10.1016/j.jhazmat.2020.123597
Received 6 April 2020; Received in revised form 26 July 2020; Accepted 27 July 2020
Available online 2 August 2020

measure various organic and inorganic elements in different environments such as water, soils and sediments (Li et al., 2019a). At present, simultaneous measurement of three types of analytes, including cations, oxyanions, and sulfides has been realized using a single binding gel containing three binding agents: Chelex-100 resin, Zr-oxide and AgI (Wang et al., 2019). The DGT-measured oxyanions include high and low valence cations, such as chromate and $Cr(OH)_2^+$ (Wang et al., 2019; Chitrakar et al., 2006; Devillers et al., 2016). Furthermore, DGT coupled to inductively coupled plasma mass spectrometry (LA-ICP-MS) can provide two-dimensional (2-D) chemical imaging of multiple elements at high resolution, including metallic cations and oxyanions (Gao et al., 2015; Warnken et al., 2004; Guan et al., 2015; Fresno et al., 2017; Valentinuzzi et al., 2015; Zhou et al., 2018; Stockdale et al., 2008), but 2-D imaging of sulfides has not been realized. It has been recognized that data obtained simultaneously using a single DGT binding layer can be easier to interpret especially for 2-D imaging, as deployment conditions and spatial resolution are congruent (Stockdale et al., 2008). However, no technique has been available for the simultaneous 2-D imaging of sulfides, metallic cations and oxyanions using a single DGT binding layer.

The precipitation/dissolution process reactions of cations, anions and sulfides are reversible and can be highly sensitive to environment conditions in sediments, such as dissolved oxygen (DO) and pH levels (Guan et al., 2015). Typically, these parameters are measured using microsensors in one spatial dimension, although this cannot allow for the assessment of the heterogeneity of sediments at a two-dimension level (Glud et al., 1996; Li et al., 2019b). The planar optrode (PO) technique was first developed for the in-situ measurement of DO in sediments at a high spatial resolution (< 100 μm) (Glud et al., 1996). Recently, this technique has been modified for the measurement of various solutes in sediments or soils, including pH, pCO_2, NH_4^+, Fe^{2+} and Mn^{2+} (Zhu, 2019). In addition, combined PO and DGT sensors have been shown to be a promising method for the simultaneous measurement of multiple analytes (Li et al., 2019b; Zhu, 2019; Kreuzeder et al., 2018; Hoefer et al., 2017; Stahl et al., 2012), and it is desirable to enable 2-D imaging of more analytes with the development of each techniques.

In this study, a new high resolution DGT (HR-ZCA DGT) was developed for simultaneous 2-D imaging of sulfides, metallic cations and oxyanions (S, Fe, P, Mn, As, W, V, Co, Ni, Zn, Mo, Sb, Cr, Cu, Pb, Cd and Se) at a submillimeter scale. All the elements were enriched in a new DGT binding gel (HR-ZCA gel), followed by LA-ICP-MS analysis. Furthermore, a hybrid sensor containing the binding gel and an O_2 planar optrode was deployed for simultaneous 2-D imaging of O_2 and the aforementioned elements in sediments.

2. Experiment

2.1. Materials and solutions

Deionized water (18.2 MΩ cm Milli-Q water, Millipore) was used to prepare solutions. Prior to use, all plastic containers and glassware were acid-cleaned in 20 % (v/v) HNO_3 for over 24 h followed by thorough rinsing with deionized water. All chemicals were supplied by the National Standard Materials Network (Beijing, China), unless otherwise stated. The binding agent Chelex-100 resin was provided by Bio-Rad (USA). Acrylamide, N, N' - methylene diacrylamide (MBA), N, N, N', N' - tetramethylethylenediamine (TEMED) and ammonium persulfate (APS) (Amresco, USA) were used for the preparation of binding gels, while agarose (Bio-Rad, USA) was used to prepare the diffusive gel. Platinum (II) 2, 3, 7, 8, 12, 13, 17, 18-octaethyl-21H, 23H-porphyrin (PtOEP) (Frontier Scientific Inc., USA), Macrolex® fluorescence yellow 10 G N (MY) (Kremer Pigments Inc., USA) and polystyrene (PS) (Sigma-Aldrich, USA) were used to prepare the O_2 planar optrode.

2.2. Preparation of DGT and hybrid PO-DGT sensors

The diffusive gel was prepared using 1.5 % (m/v) agarose according to the method reported by Wang et al. (2016) (Wang et al., 2016). The binding gel was prepared using a novel procedure as follows. A weight of 0.4 g Chelex-100 resin was ground thoroughly. 0.153 g $AgNO_3$ was dissolved in 0.45 mL deionized water. The ground Chelex-100 resin and dissolved $AgNO_3$ solution were then mixed with a 4.22 mL polyacrylamide solution, followed by the addition of 10 μL of 10 % w/w APS and 2.5 μL TEMED to form the gel solution. The gel solution was pipetted between two preheated glass plates separated by 0.40 mm thickness plastic spacers. After a 30 min polymerization period, the gel was immersed in 500 mL of 0.2 mol L^{-1} KI over 12 h. Then the gel was immersed in a solution of 16.10 g $ZrOCl_2{\cdot}8H_2O$ dissolved in 500 mL of deionized water for 2 h, followed by immersion in 500 mL of 0.05 mol L^{-1} MES (pH = 6.70) for 40 min to form the binding gel (Guan et al., 2015). The binding gel was immersed in deionized water to remove all residual chemicals and then maintained in 0.01 mol L^{-1} $NaNO_3$ before use. All preparation steps were performed in the dark, at room temperature. The diffusive gel (0.80 mm), binding gel (0.40 mm) and Durapore® PVDF membrane (0.45 μm pore size and 100 μm thickness; Millipore, USA) were assembled in a piston-type DGT unit (EasySensor Ltd., Nanjing, China) for solution deployment.

The O_2 planar optrode was prepared by dissolving 10 mg PtOEP, 10 mg MY and 500 mg PS with toluene according to the method reported by Larsen et al. (2011) (Larsen et al., 2011), with details provided in the

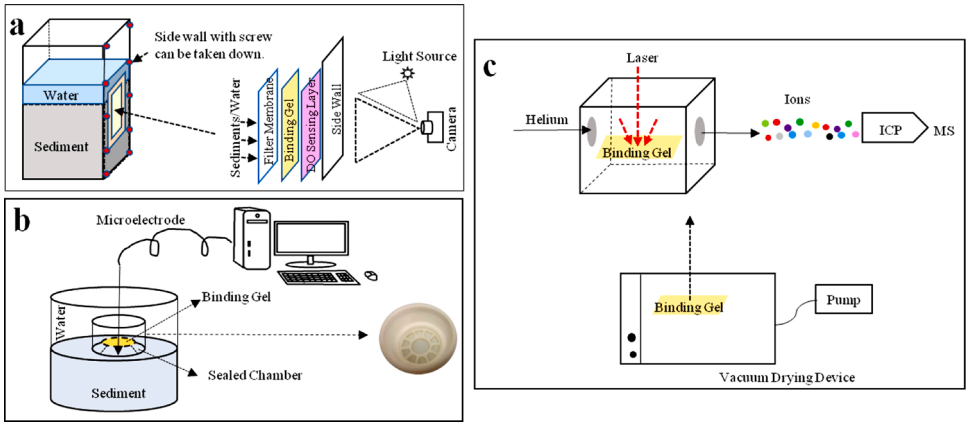

Fig. 1. (a) Diagram of the combined DGT and PO sensor; (b) Diagram of the equipment used to investigate the gas permeability of the HR-ZCA gel; (c) LA-ICP-MS analysis process diagram.

Supplementary Information (SI). The DGT binding gel was mounted onto the O_2 planar optrode (2.0 μm thickness) using tape, avoiding the formation of air bubbles. Following this, the PVDF membrane was overlaid on the DGT binding gel to protect the gel, resulting in a hybrid sensor with an overall approximate 0.50 mm thickness being formed for deployment in sediments (Fig. 1a). Planar optrode imaging was performed using a PO device (PO2100) provided by EasySensor Ltd. (Nanjing, China), with two 410−420 nm LED arrays applied as the excitation light sources. Images of the fluorescent light emitted by the optrode were captured using a CCD camera (resolution 4272 × 2848 pixels) equipped with a macro lens (Fortune Technology, China) and a 460 nm long-pass emission filter (Nmot, China).

2.3. Validation of HR-ZCA DGT in solutions

To determine the elution efficiency of the binding gel for 16 elements (all elements except S), the HR-ZCA gel was immersed in 20 mL of a mixed solution containing the 16 elements (except for S) for 24 h. Following this, the gel was retrieved and the metallic cations and oxyanions were eluted from the gel by a two-step procedure reported previously (Wang et al., 2019). Briefly, metallic cations were first eluted from the binding gel using 1.0 mol L^{-1} HNO_3, followed by elution of oxyanions using a mixture of 0.2 mol L^{-1} NaOH and 0.5 mol L^{-1} H_2O_2 (Wang et al., 2019). Comprehensive details are provided in SI. The metallic cations and oxyanions in the elution solution were detected by ICP-MS (Agilent Technologies 7700, USA). The elution efficiency of the HR-ZCA gel for the 16 elements (except for S) was calculated as the ratio between the amount eluted from the binding gel and the amount removed from the working solution by absorption.

HR-ZCA DGT was validated in solution according to the following procedure. The HR-ZCA DGT devices were immersed in 10 L of mixed solution containing the 16 elements (except for S) for 24 h. DGT devices were retrieved from the solution at time intervals of 1, 2, 6, 8, 10, 12, 17, 20 and 24 h, with measurement of the concentration of each element remaining in the solution. Additionally, the metallic cations and oxyanions were eluted from the binding gel and were measured by ICP-MS. Further details are provided in SI. The relationship between the mass of the 16 elements (except for S) accumulated in the HR-ZCA gel and deployment time, was examined for validation of the HR-ZCA DGT device.

2.4. Quantitative analysis of multiple elements using LA-ICP-MS

To test the feasibility of using LA-ICP-MS as a quantitative analytical technique, calibration standards were prepared by plotting standardized laser ablation signals of elements (signals of elements divided by signals of internal standard ^{13}C) versus the corresponding elemental mass accumulated on the binding gel per analyzed ablation spot (pg/spot) (Gao et al., 2015). The mass of multiple elements accumulated on the binding gels per analyzed ablation spot (pg/spot) (Gao et al., 2015) was calculated as follows. Total amount of element accumulated in the binding gel, per area of exposed surface (3.14 cm^2) was then multiplied by the area of the ablation spot (3.53 × 10^{-4} cm^2). For this, quadruplicate DGT devices were deployed in 2 L working solutions containing 15 elements (all elements except for Fe and S) at varying individual element concentrations of 0, 10, 20, 40, 80 and 100 μg L^{-1}. Working solutions containing 15 elements (except for Fe and S) were diluted from standard solutions (a mixture of 100 mg L^{-1} multielement standard solution for ICP analysis), with 0.004 mol L^{-1} $Mg(NO_3)_2$ added to the mixed solutions to minimize adsorptive losses. To avoid competition and precipitation reactions among multiple elements, 0.01 mol L^{-1} NaOH and 0.01 mol L^{-1} HNO_3 were added to the solutions for the adjustment of pH values to within 5.0−6.0. After 24 h of deployment, three binding gels were eluted by the two-step extraction procedure as described above (Wang et al., 2019) for the measurement of metallic cations and oxyanions by ICP-MS. The fourth gel was dried using a gel vacuum dryer prior to LA-ICP-MS analysis as follows. The gels were placed onto three layers of PVDF membranes and were covered by one layer of PVDF membrane, and then were transferred to a NZG-A type gel vacuum dryer (JUNYI Electrophoresis, Beijing, China), where they were dried at 50 °C for 3 h. In the drying process, only the gel thickness diminished, while all other dimensions were maintained. After drying, six random lines at the central position of the dried gels were selected for LA-ICP-MS analysis, with each line containing ~80 laser points. To test the precision of LA-ICP-MS analysis, average and relative standard deviation (RSD) values of the standardized laser ablation signals for the six random lines of each gel were calculated.

Due to its easy oxygenation and precipitation in solution, working solutions of Fe(II) were prepared separately and Fe(II) was measured by phenanthroline colorimetric methods (Xu et al., 2013) using an Epoch Microplate Spectrophotometer (BioTek, USA). In addition, working solutions of sulfide were also prepared separately due to its easy oxygenation and precipitation. After retrieval of the binding gels, three binding gels were processed to measure the accumulated sulfide mass according to the method reported by Teasdale et al. (1999) (Teasdale et al., 1999). A fourth gel was dried as mentioned above for further LA-ICP-MS analysis.

After drying, the binding gel was mounted onto glass microscope slides using double-sided adhesive tape, avoiding uneven surface caused by air bubbles and was then further ablated. An ASI RESOLution-LR-S155 laser microprobe equipped with a Coherent Compex-Pro 193 nm ArF excimer laser was used for laser sampling, with ion-signal intensities obtained using an Agilent 7700x ICP-MS instrument. To improve analytical precision, the ^{13}C, which is the major elemental component of the matrix of the binding gel, was used as an internal normalization standard as proposed by Lehto et al. (2012) (Lehto et al., 2012). The operating conditions for LA and ICP-MS analysis are summarized in Table 1.

2.5. DGT-PO hybrid sensor tests

2.5.1. Gas permeability of the binding gel

For the hybrid sensor, O_2 passing through the DGT binding gel is captured by the O_2 planar optrode. Accordingly, application of the hybrid sensor requires that the DGT binding gel should be gas permeable. A device was designed to investigate the gas permeability of the binding gel (Fig. 1b), consisting of a base, a ring-shaped cover and a binding gel. The groove at the top of the base was hollow to ensure that gas could pass through. The binding gel was placed in the groove and was fixed by the ring-shaped cover. The groove is hollow and the cover is ring-shaped, resulting in both sides of the binding gel being exposed to O_2. When the device was upended on the sediment surface, a chamber formed between the exposed surface of the binding gel and the sediment. Accordingly, the gas permeability of the binding gel could be investigated by measuring the change of O_2 concentration in the chamber (Fig. 1b).

The device containing a binding gel was deployed in a sediment core with overlying water (10 cm depth) above the sediment-water interface (SWI). Initial O_2 concentrations in the overlying water were ~5.5 mg

Table 1
Operating parameters of the LA-ICP-MS system.

LA		ICP-MS	
Laser spot size	188μm	transport gas (Ar) flow rate	900 mL/min
Distance between lines	0	Internal standard	^{13}C
Scanning speed	50 μm/s		
Acquisition time	0.006 s		
Repetition rate	10 Hz		
Energy output	2.5 J/cm^2		
Carrier gas (He) flow rate	300 mL/min		

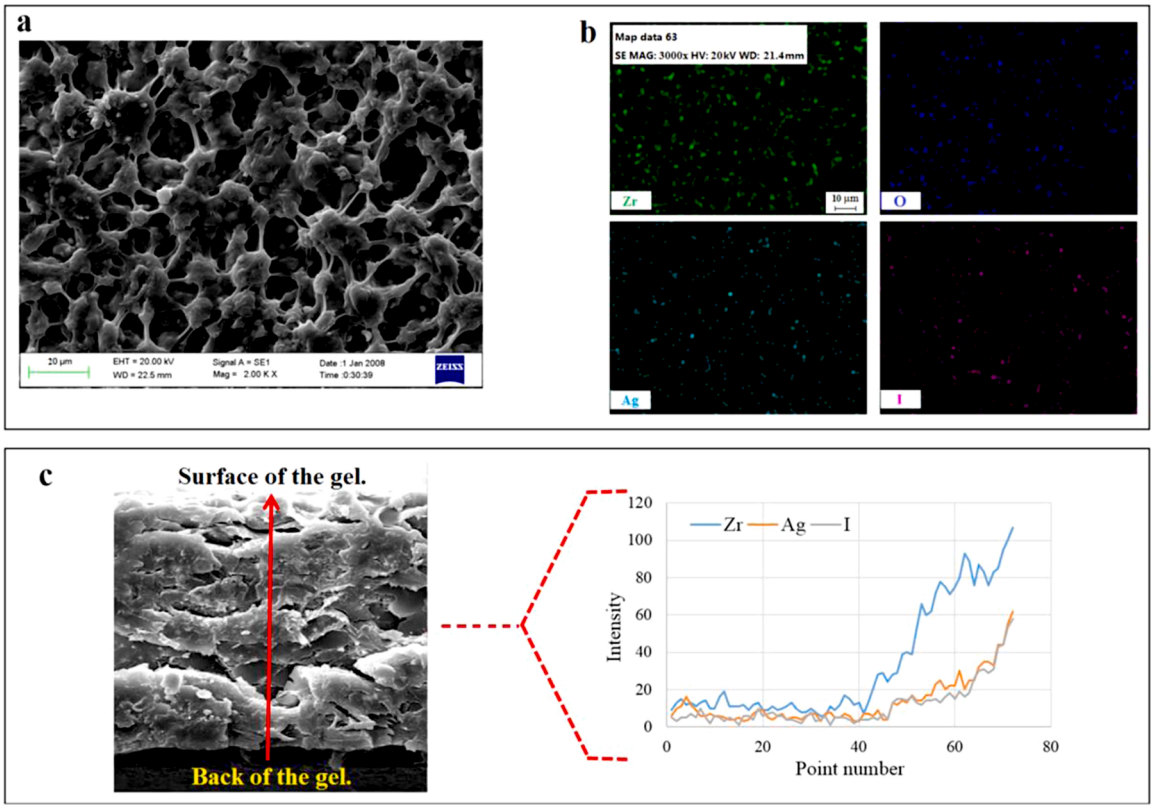

Fig. 2. SEM-EDS images of the HR-ZCA binding gel. (a) Surface image of the binding gel; (b) Distribution of elements in the binding gel; (c) Cross-section image of the binding gel, with the red arrow indicating the direction from the back to the surface of the binding gel.

L^{-1}. The changes in O_2 concentrations in the chamber during 170 min of deployment were measured at 5 min intervals using a microelectrode (Unisense, Denmark).

2.5.2. Calibration of the planar optrode

The calibration process for the planar optrode in the hybrid sensor was carried out according to the method previously reported by Christel et al. (2016) (Christel et al., 2016). The 2 × 2 cm hybrid sensor was attached to the inside wall of a transparent Perspex box (10 × 10 × 20 cm). Deionized water was added to the box and the hybrid sensor was immersed in water. Planar optrode imaging was conducted under varying dissolved oxygen levels, adjusted using an air pump (Eheim, Germany). The equilibrium time is the time needed that fluorescence intensity of the planar optrode reaches stability. Considering the thickness of the hybrid sensor, a 10 min equilibration time was adopted. Detailed methodology is provided in SI.

2.5.3. Sediment measurements

Sediment cores and overlying water were collected from Meiliang Bay (31°26′18′′ N, 120°11′12′′ E), in the northern part of Lake Taihu (Jiangsu, China). Sediment cores were sectioned at 2-cm intervals and were placed in the transparent Perspex box according to their original depth. Next, the boxes were put into a tank containing a 35 cm depth of filtered lake water. The water was oxygenated for two weeks to create aerobic conditions and after two weeks of incubation, one sidewall of the boxes was removed and the hybrid sensor was attached to it and was exposed to the transparent window (Fig. 1a). The boxes were then allowed to continue incubating for 24 h under aerobic conditions and during this period, fluorescent images were recorded at 8 -h intervals. After 24 h of deployment, the hybrid sensor was retrieved. Before drying of the binding gel for LA-ICP-MS analysis, the 2-D distribution of sulfides were obtained using the CID method previously reported by Wang et al. (2019) (Wang et al., 2019). Additionally, the 2-D image of sulfide obtained by LA-ICP-MS analysis was compared with the image using the CID technique. All experiments were carried out at 25 °C and the process diagram is presented in Fig. 1c.

2.5.4. Sample analysis and calculation

Scanning electron microscopy (SEM) and energy dispersive analysis (EDS) (ZEISS EVO 18, Germany) were used to characterize the dried binding gel for investigation of the distribution of binding agents in the binding gel. The 2-D distribution of DGT-labile sulfide fluxes was obtained using the CID method according to the method reported by Wang et al. (2019) (Wang et al., 2019). The binding gel was scanned using a CanoScan 9000F-type scanner. Based on the scanned images, the areas of interest in the binding gel were processed using Image J software. The 2-D distribution of DGT-labile fluxes of all 17 elements were obtained using LA-ICP-MS and Iolite 4.0 software, with further smoothing performed using the image smoothing function of Photoshop software.

The mass of target solutes accumulated on binding gels (M, ng) were calculated according to the method reported by Zhang et al. (1995) (Eq. S2) (Zhang and Davison, 1995). The DGT-measured concentration (C_{DGT}, $mg \cdot L^{-1}$) of target solutes were also calculated according to the Zhang et al. (1995) method (Eq. S3) (Zhang and Davison, 1995). The diffusion coefficients ($cm^2 \cdot s^{-1}$) of analytes were applied as cited by Wang et al. (2016) (Wang et al., 2016). The mean flux (F, $\mu g \cdot cm^{-2} \cdot s^{-1}$) of DGT-labile element fractions were calculated according to the method reported by Li et al. (2019) (Eq. S4) (Li et al., 2019a).

Pearson correlation analysis was performed using SPSS 16.0 software, for the evaluation of significant correlations between parameters.

3. Results and discussion

3.1. SEM-EDS images of the binding gels

Effective coupling of the DGT technique with LA-ICP-MS analysis,

Table 2
Elution efficiency of the HR-ZCA binding gel for 16 elements (except for S). Values represent the mean ± SD of three replicates.

Element	Elution efficiency (%)	Element	Elution efficiency (%)
Mn	91.8 ± 1.25	V	92.1 ± 3.43
Co	94.1 ± 2.38	Cr	99.1 ± 1.54
Ni	95.6 ± 1.44	As	99.2 ± 1.05
Cu	90.2 ± 1.87	Se	99.7 ± 1.02
Zn	88.7 ± 2.21	Mo	97.5 ± 2.39
Cd	95.9 ± 1.07	Sb	98.0 ± 2.85
Pb	99.2 ± 1.69	W	94.2 ± 3.42
Fe	88.8 ± 1.92	P	87.6 ± 2.08

requires that binding agents in the binding gel should be small enough (≤10 μm) to ensure minimal variation in the distribution of binding sites for analytes (Guan et al., 2015). To investigate the distribution of the three binding agents in the binding gel, the vacuum dried gel was characterized by SEM-EDS, with the cross-linked structure observed in the binding gel (Fig. 2a). Furthermore, the signal intensities of Zr, Ag and I elements exhibited peak values in the region of the gel surface (Fig. 2c), indicating that Zr-oxide and AgI were enriched on the upper surface of the binding gel. The surface image of the binding gel confirmed that Zr, Ag, I and O elements were distributed evenly (Fig. 2b). Since O is a major elemental component of Chelex-100 resin (Yabutani et al., 1999), it indicates that Zr-oxide, AgI and the Chelex-100 binding agent were all evenly distributed on the surface of the binding gel.

3.2. Elution efficiencies of the binding gel

The elution efficiencies of the HR-ZCA gel for 16 elements (except for S) are listed in Table 2, with the elution efficiency for Se being the highest (99.7 %) and that for P being the lowest (87.6 %). The elution efficiencies of the HR-ZCA gel were compared with the corresponding values from previously reported literature on ZrO-CA gels containing the same binding agents (Wang et al., 2019). The elution efficiency of the HR-ZCA gel for Co, Ni, Cu, Cr, Se, Zn, Cd, Pb, Mo, W, Fe and P were similar to the previously reported ZrO-CA gel values. In contrast, the elution efficiencies of the HR-ZCA gel for As, Sb and V (99.2 %, 98.0 % and 92.1 %, respectively) were much higher than those previously reported for ZrO-CA gels (76.2 %, 54.3 % and 55.1 %, respectively) (Wang et al., 2019).

3.3. Validation of HR-ZCA DGT in solutions

The HR-ZCA DGT device was validated by examining the relationship between the masses of all 16 elements (except for S) accumulated in the HR-ZCA gel and the deployment time, with results shown in Fig. 3. The measured mass of each element was calculated using Eq. S2, with results showing that all increased linearly with time throughout the deployment period (R^2 for all 16 elements >0.997). The experimental data agreed well with the theoretical predicted values calculated using Eq. S3, with the measured/predicted ratio for all 16 elements being between 0.99 and 1.02, validating the use of the HR-ZCA gel for DGT measurement.

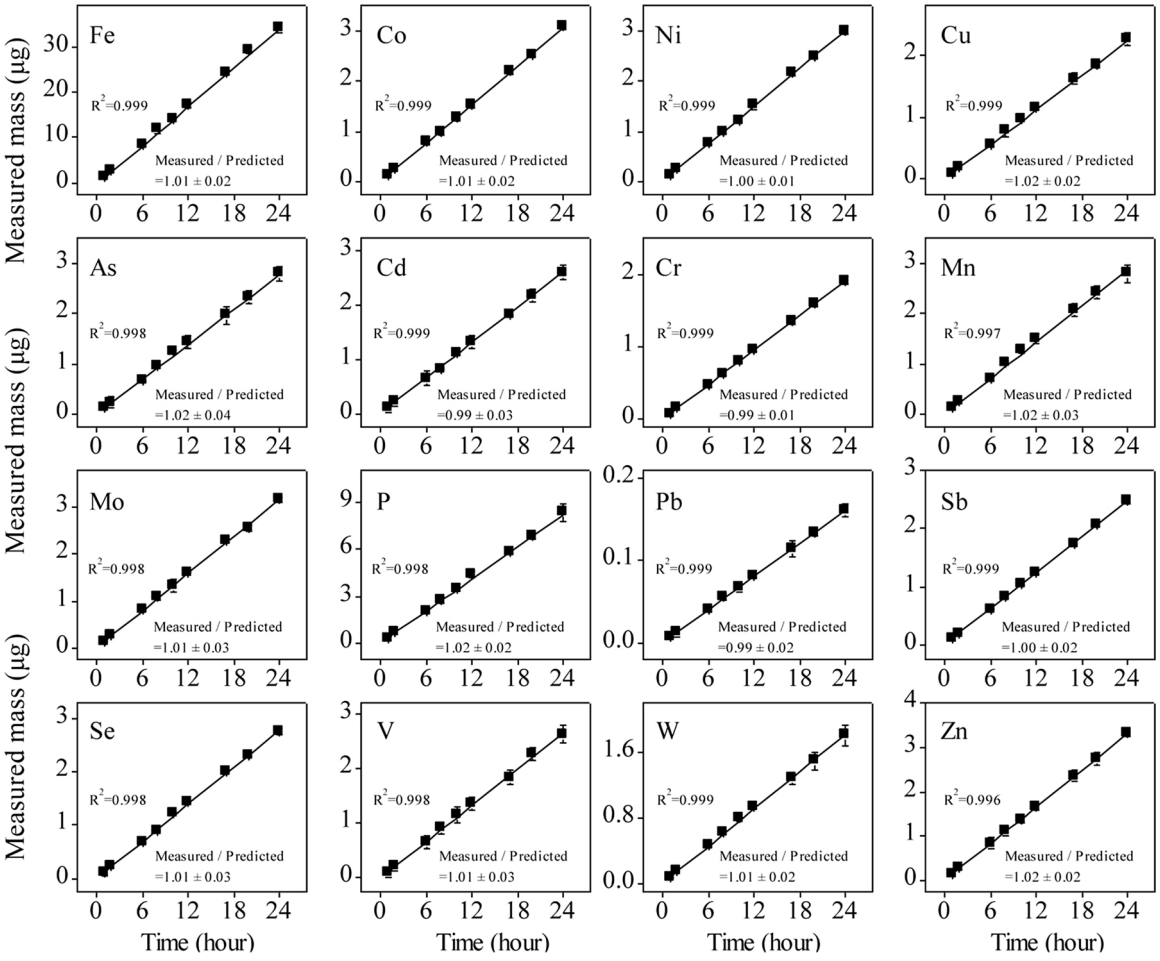

Fig. 3. Relationships between the accumulated mass of each element in HR-ZCA DGT devices with deployment time.

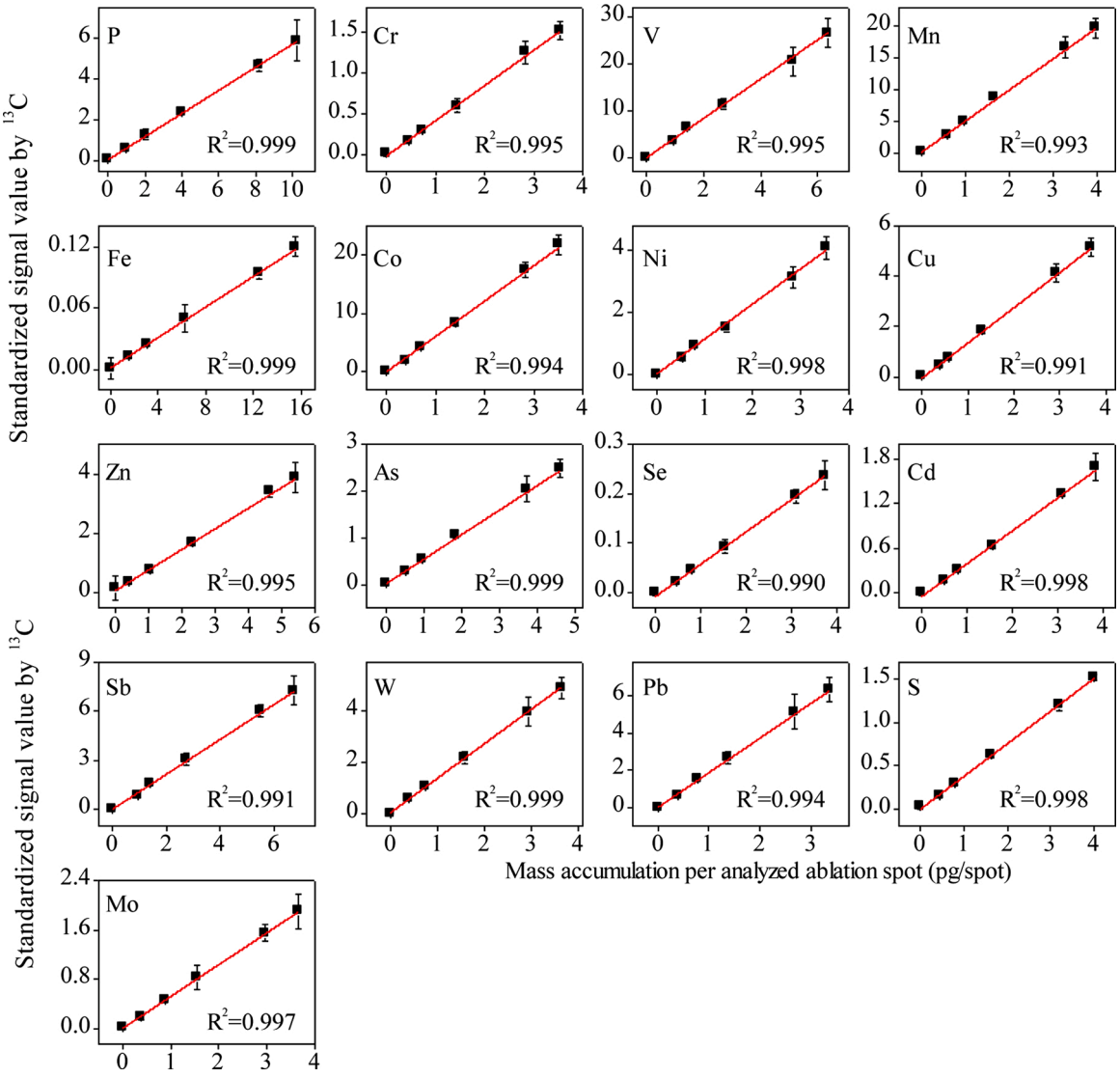

Fig. 4. Standardized laser ablation signals for all assessed elements, plotted versus the accumulated mass on binding gels per analyzed ablation spot (pg/spot).

Table 3
Average and RSD (%) values of standardized laser ablation signals (element signal divided by the internal standard ^{13}C signal) of six random lines on gels deployed in six different working solutions.

Element	Working solution 1		Working solution 2		Working solution 3		Working solution 4		Working solution 5		Working solution 6	
	Average	RSD	Average	RSD	Average	RSD	Average	RSD	Average	RSD	Average	RSD
V	0.02	8.0	3.2	4.2	6.67	2.9	14.0	8.6	28.9	11.6	33.3	9.2
Cr	0.02	4.1	0.2	8.5	0.4	8.3	0.8	11.1	1.6	8.4	1.4	8.5
Mn	0.17	10.7	2.1	5.3	3.7	2.8	8.5	3.6	20.9	8.5	19.9	8.4
Co	0.002	4.3	2.2	4.2	4.4	1.3	9.2	8.1	19.8	6.3	24.1	7.4
Ni	0.007	2.9	0.6	10.9	0.9	2.9	1.8	8.3	4.0	8.7	4.7	8.1
Cu	0.04	5.2	0.4	7.1	0.9	3.4	1.8	8.8	4.1	9.5	4.8	7.0
Zn	0.16	3.9	0.9	7.3	0.9	8.4	1.9	4.4	2.4	7.3	4.04	10.0
As	0.01	1.6	0.3	5.5	0.6	1.3	1.2	7.3	2.6	10.8	2.9	7.9
Se	0.001	5.0	0.03	4.6	0.06	2.7	0.1	12.2	0.2	8.4	0.3	11.0
Mo	0.015	2.0	0.5	6.9	1.0	2.7	1.1	2.1	1.4	10.7	2.5	9.1
Cd	0.01	4.0	0.2	7.8	0.4	3.6	0.6	6.8	1.4	2.1	1.9	9.3
Sb	0.014	1.7	1.0	6.3	2.2	3.2	4.0	9.6	8.2	5.5	8.7	10.9
W	0.001	7.0	0.7	7.6	1.4	2.9	2.9	9.1	5.1	11.7	4.8	8.6
Pb	0.004	9.2	1.1	5.4	2.2	4.5	4.4	7.2	9.2	10.6	7.8	8.8
P	0.07	5.2	0.7	4.1	1.3	5.6	2.6	3.6	5.1	10.0	6.0	2.7
Fe	0.003	10.2	0.01	7.9	0.02	6.3	0.04	6.6	0.09	5.4	0.1	6.5
S	0.02	2.3	31.0	8.6	37.0	4.1	44.0	6.5	58.0	7.0	61.0	9.6

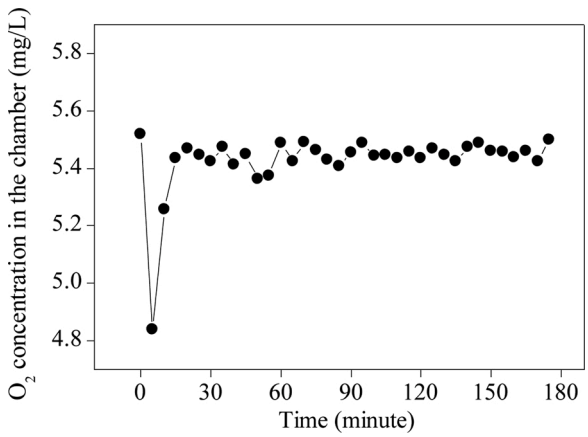

Fig. 5. Change in O_2 concentration in the chamber formed between the exposed surface of the binding gel and the sediment surface.

3.4. Analytical performance of LA-ICP-MS

Calibration standards were prepared for the quantitative calculation of multiple elements in the binding gel using LA-ICP-MS analysis. Standardized laser ablation signals (element signals divided by internal standard ^{13}C signals) for all 17 elements were plotted versus their accumulated mass on binding gels per analyzed ablation spot (pg/spot), with the generated curves provided in Fig. 4. A good linear relationship (R^2 for all 17 elements >0.99) was observed between the accumulated mass on binding gels and the corresponding standardized laser ablation signal, confirming the feasibility of use of LA-ICP-MS as a quantitative analysis technique for DGT measurement.

To assess the precision of LA-ICP-MS analysis, average and relative standard deviation (RSD) values of the standardized laser ablation signals of six random lines on the gels deployed in different working solutions were calculated, with the results listed in Table 3. Good analytical precision was achieved for all 17 elements with most of the RSD values being less than 10 % and the lowest being 1.3 %. The highest RSD value in this study was 12.2 % (for Se) which was similar to the highest values previously reported in the literature of 10.5 % (for Ni) (Wang et al., 2019) and 9.9 % (for As) (Stockdale et al., 2008).

3.5. Gas permeability of the binding gel for DGT-PO measurement

To investigate the gas permeability of the binding gel capable of PO measurement, the binding gel containing device was upended on the sediment surface (Fig. 1b). Changes in O_2 concentrations in the chamber over time were measured and the results are shown in Fig. 5. In the first 5 min, O_2 concentrations in the chamber decreased from ~5.5 mg L^{-1} to ~4.8 mg L^{-1} likely due to consumption of O_2 by various processes occurring at the sediment surface. Following this, O_2 concentrations in the chamber increased from ~4.8 mg L^{-1} at the end of 5th minute to ~5.2 mg L^{-1} at the end of 10th minute and remained at ~5.4 mg L^{-1} thereafter. Results demonstrated that the HR-ZCA binding gel was gas permeable and could effectively be coupled with the O_2 planar optrode to form a hybrid sensor for the simultaneous measurement of multiple elements and O_2 concentrations.

3.6. Distribution of multiple elements and O2 in sediments measured using the hybrid DGT-PO sensor

The 2-D distribution of DGT-labile fluxes of all 17 elements based on LA-ICP-MS analysis and 2-D imaging of O_2 concentrations at the end of the 24 h deployment time are shown in Fig. 6. The 1-D distribution of DGT-labile fluxes of all 17 elements and 1-D imaging of O_2 concentrations were mapped, as shown in Fig. 7. The fluxes of Se measured by LA-ICP-MS analysis were mostly very low. As a result, other elements except Se, were mainly discussed in the following discussion.

The CID method has been used for 2-D imaging of sulfide in previously reported literature. The inclusion of sulfide measurements by LA-ICP-MS analysis is desirable for the easy interpretation of results, as the resolution and measurement conditions are comparable to the other elements. To demonstrate the utility of LA-ICP-MS analysis for the

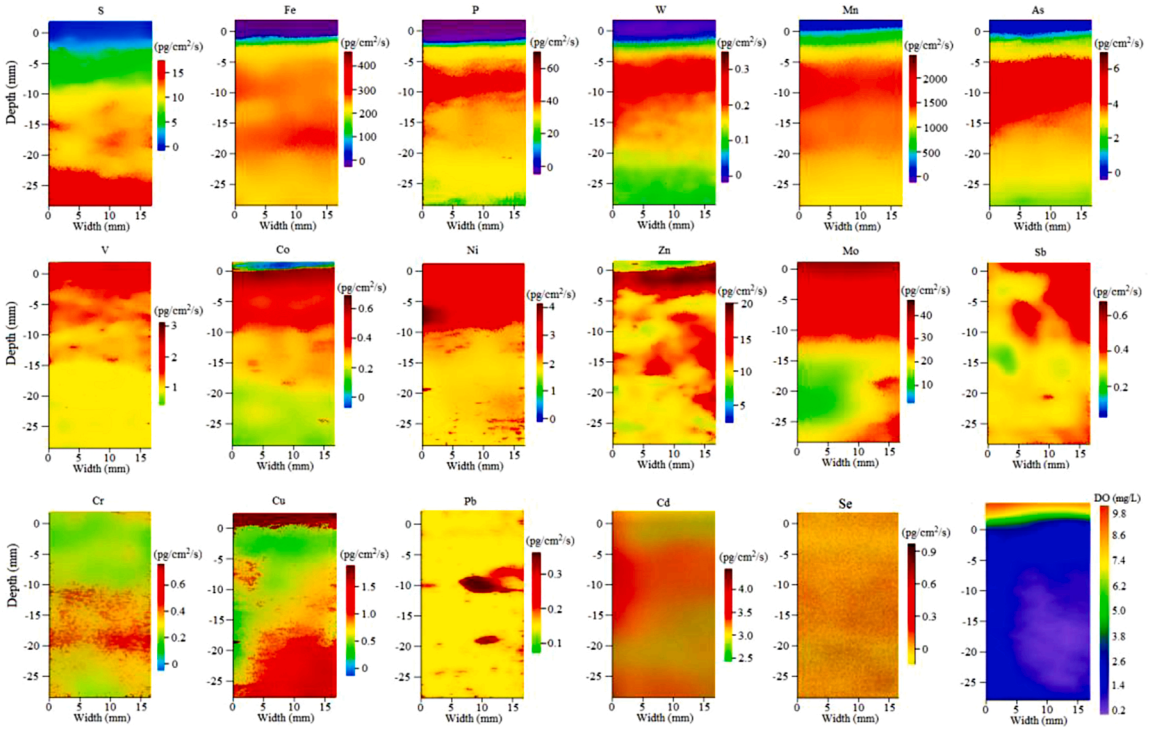

Fig. 6. 2-D distribution of DGT-labile fluxes of all 17 elements with LA-ICP-MS analysis and 2-D imaging of O_2 concentrations.

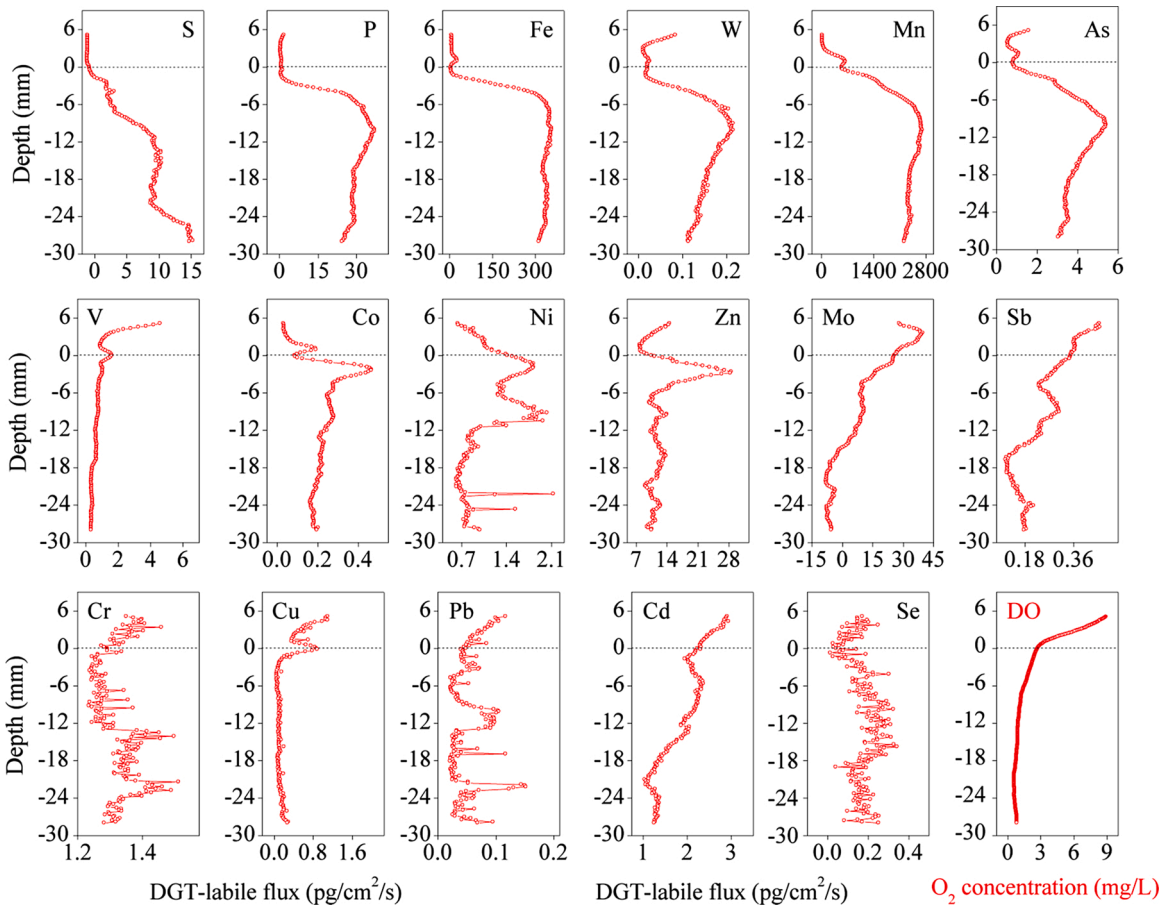

Fig. 7. 1-D vertical distribution of DGT-labile fluxes of all 17 elements at a 0.188 mm resolution and 1-D distribution of O_2 concentrations at a 0.079 mm resolution.

quantitative calculation of sulfide fluxes, the results obtained by LA-ICP-MS analysis were compared with results obtained using the CID method. The distribution of DGT-labile sulfide fluxes obtained using the CID method is shown in Fig. S1. 2-D and 1-D sulfide distributions obtained by LA-ICP-MS analysis were found to be similar with those obtained using the CID method. In addition, from 5 mm above the SWI to a sediment depth of −28 mm, fluxes of sulfide measured using LA-ICP-MS analysis ranged from ~0 to ~15.3 $pg \cdot cm^{-2} \cdot s^{-1}$, which were similar to those determined using the CID method (ranging from ~0 to ~12.5 $pg \cdot cm^{-2} \cdot s^{-1}$). It has previously been reported that a change in sulfide concentrations cannot be reflected when the gray scale exceeds 255, as a result, the CID method are subject to the coloration of the gel while laser ablation analysis are not (Wang et al., 2019). Accordingly, LA-ICP-MS analysis was confirmed to be a more suiTable 2 -D imaging technique and the sulfide data obtained by LA-ICP-MS analysis was used for all further discussion.

In sediments, metals and metalloids can be adsorbed onto, or co-precipitated by Fe/Mn oxides and sulfides, resulting in their mobility depending on the redox potential of sediments and exhibits different responses for varying sediment types with different characteristics (Banks et al., 2012). The redox conditions in sediments are usually stratified and zones are frequently referred to as being oxic, sub-oxic, or anoxic (Nelson et al., 2004; Preisler et al., 2007). The oxic zone occurs at the sediment surface with high O_2 levels of penetration into the sediment surface. The sub-oxic zone is the zone in which Fe/Mn oxides serve as electron donors for organic matter mineralization and sulfide oxidation. The sulfidic zone is the boundary layer in which sulfide produced from the reduction of sulfate diffuses from the deeper sulfate zone (Nelson et al., 2004).

P, W, As, Fe and Mn exhibited highly similar distribution patterns in the sediment profile (Figs. 6 and 7). In addition, correlation between 17 elements fluxes were analyzed and results showed that P, W and As were all significantly positively correlated ($p < 0.01$) with Fe and Mn (Table 4). These results demonstrate that the mobility of P, W and As are controlled by Fe/Mn oxides. The fluxes of these five elements were small at the sediment surface, while increased to higher values from a sediment depth of 5 mm–20 mm. The small flux values for Fe, Mn, P, W and As at the sediment surface may be because in the upper oxic zone, manganese and iron occur mostly in oxidized mineral phases and trace elements complexed with Fe/Mn oxides may not be measured (Hongve, 1997). However, with deeper depths into the sub-oxic zone, Fe/Mn oxides serve as oxidants in the mineralization of organic matter, causing an increase in Fe(II)/Mn(II) with increasing depth when reduction occurs. As a result, the adsorbed and coprecipitated trace elements by Fe/Mn oxides are released into the pore water, causing an increase in the flux of Fe, Mn, P, W and As (Ding et al., 2016; Chen et al., 2018).

Correlation analysis results showed that significant positive correlations ($p < 0.01$) were found between V, Co, Ni, Zn, Mo, Cd and Sb (Table 4). In contrast to Fe, Mn, P, W and As, the fluxes of V, Co, Ni, Zn, Mo, Cd and Sb were high at the sediment surface, indicating that the mobility of these elements was not controlled by Fe/Mn oxide precipitation/dissolution processes. It has previously been indicated that the oxidation of iron sulfides by oxygen in sediment environments and the generation of SO_4^{2-} as a product, occurs via a rapid process, with trace elements coprecipitated along with iron sulfides and released at the sediment surface (Morse, 1991; Moses and Herman, 1991). In addition, oxidized iron was significantly enhanced at the sediment surface which also suggests a major fraction of Fe^{2+} is produced due to iron sulfide dissolution (Naylor et al., 2004). In this study, V, Co, Ni, Zn, Mo, Cd and Sb all exhibited a significant and negative correlation ($p < 0.01$) with S

Table 4
Correlations between DGT-labile fluxes of all 17 elements from a sediment depth of 0 mm to −28 mm. (* and ** indicate that correlations are significant at the 0.05 and 0.01 level, respectively).

	P	S	V	Cr	Mn	Fe	Co	Ni	Cu	Zn	As	Se	Mo	Cd	Sb	W	Pb
P	1																
S	0.031	1															
V	0.17	−0.886**	1														
Cr	0.173*	0.384**	−0.393**	1													
Mn	0.967**	0.011	0.05	0.208**	1												
Fe	0.943**	0.206*	−0.236**	0.286**	0.897**	1											
Co	−0.27**	−0.886**	0.881**	−0.437**	−0.207**	−0.481**	1										
Ni	0.77	−0.758**	0.731**	−0.461**	0.1	−0.126	0.704**	1									
Cu	−0.215**	0.662**	−0.61**	0.054	−0.204*	−0.112	−0.567**	−0.315**	1								
Zn	−0.607**	−0.68**	0.676**	−0.282**	−0.546**	−0.75**	0.842**	0.435**	−0.344**	1							
As	0.836**	−0.368**	0.471**	−0.062	0.876**	0.636**	0.242**	0.443**	−0.427**	−0.163*	1						
Se	0.234**	−0.005	0.178*	−0.044	0.248**	0.131	0.039	0.087	−0.021	−0.039	0.309**	1					
Mo	−0.004	−0.834**	0.907**	−0.521**	0.002	−0.265**	0.826**	0.797**	−0.487**	0.551**	0.434**	0.145	1				
Cd	0.253**	−0.837**	0.925**	−0.451**	0.226**	0.009	0.765**	0.754**	−0.593**	0.436**	0.628**	0.203*	0.912**	1			
Sb	0.031	−0.669**	0.677**	−0.578**	0.046	−0.187*	0.589**	0.801**	−0.163*	0.322**	0.37**	0.115	0.870**	0.769**	1		
W	0.925**	−0.281**	0.35**	0.018	0.923**	0.783**	0.86	0.331**	−0.439**	−0.329	0.958**	0.245**	0.307**	0.539**	0.25**	1	
Pb	0.11	−0.078	0.037	0.024	0.131	0.135	0.074	0.236	0.068	0.027	0.206*	0.066	0.16*	0.022	0.154	0.118	1

(Table 4). The mobility of these elements increased with the decrease in sulfide flux, with O_2 concentrations showing relatively high values at the sediment surface (Figs. 6 and 7). These results indicate that high mobility of V, Co, Ni, Zn, Mo, Cd and Sb at the sediment surface may occur due to the oxidation of iron sulfides by oxygen.

It can be seen from the 2-D distribution figure that from a sediment depth of -20 mm to -25 mm, the DGT-labile fluxes of Ni, Zn, Mo and Sb showed nearly simultaneous local increases (Fig. 6). However, this simultaneous local increase cannot be seen in the 1-D distribution results, which highlights the advantage of LA-ICP-MS analysis for better understanding sediment geochemistry (Fig. 7). Previous studies have indicated that sulfide enters the sub-oxic zone by local sulfate reduction or by diffusion upwards from the sulfidic zone and is then rapidly consumed by Fe(III) at the interface of the sub-oxic zone and sulfidic zone (Nelson et al., 2004; Preisler et al., 2007). In this study, the local (from a sediment depth of -20 mm to -25 mm) increase in fluxes of Ni, Zn, Mo and Sb may occur due to the oxidation of sulfide by Fe(III), thus releasing trace elements complexed with sulfides. In addition, from a sediment depth of −12 mm to -20 mm, DGT-labile fluxes of S, V, Co and Zn showed nearly simultaneous local increases (Fig. 6). However, this simultaneous local increase cannot be seen in the 1-D distribution results (Fig. 7). It has previously been reported, that sulfide is consumed by Fe (III) at the interface of the sub-oxic zone and the sulfidic zone with a fraction of Fe(II) escaping into the sub-oxic zone (Teasdale et al., 1999; Banks et al., 2012) and in the absence of oxygen, the escaped Fe(II) is rapidly oxidized by Mn oxides. Furthermore, S° generated during oxidation may be microbial disproportionated to sulfide and sulfate, leading to an increase in S(II) (Aller and Rude, 1988). The local increase in fluxes of S, V, Co and Zn from a sediment depth of −12 mm to -20 mm, may occur due to the oxidation of iron sulfide causing a release of elements, while sulfide is regenerated for further cycling.

Correlation analysis results showed that DGT-labile fluxes of Cr and Cu both exhibited significant positive correlations ($p < 0.01$) with DGT-labile fluxes of S (Table 4), indicating that the mobility of Cu and Cr may be partially influenced by sulfide. However, other factors may also control their mobility as neither exhibited an obvious similarity in distribution compared with other elements. DGT-labile fluxes of Pb had significant positive correlations ($p < 0.05$) with As and Mo across the whole sediment profile (Table 4). In addition, DGT-labile Pb fluxes showed peak values at a sediment depth of -10 mm (Figs. 6 and 7), at the same position where the peak value of Fe, Mn, As, P and Mo appeared. Overall, these findings highlight that the main factors controlling the mobility of Pb remains unclear and further investigation is required.

4. Conclusions

The novel HR-ZCA DGT can simultaneously measure Cd, Co, Cu, Ni, Pb, Zn, As, Cr, Mo, Sb, Se, V, W, Mn, Fe, S and P, at high resolution (188 μm × 188 μm) using LA-ICP-MS analysis. The three fine particle size binding agents: Chelex-100 resin, Zr-oxide and AgI, were dispersed homogeneously in the binding gels. A good linear relationship (R^2 >0.99) was observed between the mass accumulated on the binding gel for the 17 elements and the corresponding standardized laser ablation signals, indicating the feasibility of using LA-ICP-MS as an effective quantitative analysis technique. Furthermore, a hybrid sensor comprising the novel DGT binding gel overlying an O_2 planar optrode was deployed in sediments for simultaneous high resolution 2-D imaging of sulfides, metallic cations, oxyanions and DO. According to the 2-D imaging results, P, W, As, Fe and Mn showed a similar simultaneous distribution pattern. In addition, nearly simultaneous local increases in some elements (Ni, Zn, Mo and Sb or S, V, Co and Zn) could be shown in the 2-D distribution images, while these were not shown in the 1-D distribution images. These results undoubtedly confirm that use of the hybrid sensor can effectively improve our understanding of sediment geochemistry and elemental dynamics.

CRediT authorship contribution statement

Mingyi Ren: Conceptualization, Methodology. **Shiming Ding:** Conceptualization, Methodology. **Zhihui Dai:** Data curation, Writing - original draft. **Jingfu Wang:** Writing - review & editing. **Cai Li:** Investigation. **Zhilin Zhong:** Software, Validation. **Jingxin Cao:** Software, Validation. **Liyuan Yang:** Validation. **Daniel C.W. Tsang:** Writing - review & editing. **Shiwei Xu:** Investigation. **Chenye Yang:** Investigation. **Yan Wang:** Software, Validation.

Declaration of Competing Interest

No conflicts of interest exist in the submission of this manuscript, the publication of which has been approved by all authors.

Acknowledgments

This research work was financially supported by the National Key Research and Development Plan (2018YFA0903003), National Natural Science Foundation of China (41621002, 41701570, 41877492 and 41701568), CAS Interdisciplinary, Innovation Team, and Research instrument and equipment, and Development Project of the Chinese Academy of Sciences (YJKYYQ20170016).

Appendix A. Supplementary data

Supplementary material related to this article can be found, in the online version, at doi:https://doi.org/10.1016/j.jhazmat.2020.123597.

References

Aller, R.C., Rude, P.D., 1988. Complete oxidation of solid phase sulfides by manganese and bacteria in anoxic marine sediments. Geochim. Cosmochim. Acta 52, 751–765.
Amrane, C., Bouhidel, K., 2019. Analysis and speciation of heavy metals in the water, sediments, and drinking water plant sludge of a deep and sulfate-rich Algerian reservoir. Environ. Monit. Assess. 191, 73.
Banks, J.L., Ross, D.J., Keough, M.J., Eyre, B.D., Macleod, C.K., 2012. Measuring hypoxia induced metal release from highly contaminated estuarine sediments during a 40 day laboratory incubation experiment. Sci. Total Environ. 420, 229–237.
Chen, M., Ding, S., Chen, X., Sun, Q., Fan, X., Lin, J., Ren, M., Yang, L., Zhang, C., 2018. Mechanisms driving phosphorus release during algal blooms based on hourly changes in iron and phosphorus concentrations in sediments. Water Res. 133, 153–164.
Chitrakar, R., Tezuka, S., Sonoda, A., Sakane, K., Ooi, K., Hirotsu, T., 2006. Selective adsorption of phosphate from seawater and wastewater by amorphous zirconium hydroxide. J. Colloid Interface Sci. 297, 426–433.
Christel, W., Zhu, K., Hoefer, C., Kreuzeder, A., Santner, J., Bruun, S., Magid, J., Jensen, L.S., 2016. Spatiotemporal dynamics of phosphorus release, oxygen consumption and greenhouse gas emissions after localised soil amendment with organic fertilisers. Sci. Total Environ. 554, 119–129.
Davison, W., Zhang, H., 1994. In situ speciation measurements of trace components in natural waters using thin-film gels. Nature 367, 546.
Devillers, D., Buzier, R., Simon, S., Charriau, A., Guibaud, G., 2016. Simultaneous measurement of Cr(III) and Cr(VI) in fresh waters with a single Diffusive Gradients in Thin Films device. Talanta 154, 533–538.
Di Toro, D.M., Mahony, J.D., Hansen, D.J., Scott, K.J., Hicks, M.B., Mayr, S.M., Redmond, M.S., 1990. Toxicity of cadmium in sediments: the role of acid volatile sulfide. Environmental Toxicology and Chemistry: An International Journal 9, 1487–1502.
Ding, S., Wang, Y., Wang, D., Li, Y.Y., Gong, M., Zhang, C., 2016. In situ, high-resolution evidence for iron-coupled mobilization of phosphorus in sediments. Sci. Rep. 6, 24341.
Fresno, T., Peñalosa, J.M., Santner, J., Puschenreiter, M., Moreno-Jiménez, E., 2017. Effect of Lupinus albus L. Root activities on As and Cu mobility after addition of iron-based soil amendments. Chemosphere 182, 373–381.
Gao, Y., van de Velde, S., Williams, P.N., Baeyens, W., Zhang, H., 2015. Two dimensional images of dissolved sulphide and metals in anoxic sediments by a novel DGT probe and optical scanning techniques. Trends Analyt. Chem. 66, 63–71.
Glud, R.N., Ramsing, N.B., Gundersen, J.K., Klimant, I., 1996. Planar optrodes: a new tool for fine scale measurements of two-dimensional O2 distribution in benthic communities. Mar. Ecol. Prog. Ser. 140, 217–226.
Guan, D.X., Williams, P.N., Luo, J., Zheng, J.-L., Xu, H.C., Cai, C., Ma, L.Q., 2015. Novel precipitated zirconia-based DGT technique for high-resolution imaging of oxyanions in waters and sediments. Environ. Sci. Technol. 49, 3653–3661.
Hoefer, C., Santner, J., Borisov, S.M., Wenzel, W.W., Puschenreiter, M., 2017. Integrating chemical imaging of cationic trace metal solutes and pH into a single hydrogel layer. Anal. Chim. Acta 950, 88–97.
Hongve, D., 1997. Cycling of iron, manganese, and phosphate in a meromictic lake. Limnol. Oceanogr. 42, 635–647.
Khademi, H., Gabarrón, M., Abbaspour, A., Martínez-Martínez, S., Faz, A., Acosta, J.A., 2019. Environmental impact assessment of industrial activities on heavy metals distribution in street dust and soil. Chemosphere 217, 695–705.
Kreuzeder, A., Santner, J., Scharsching, V., Oburger, E., Hoefer, C., Hann, S., Wenzel, W. W., 2018. In situ observation of localized, sub-mm scale changes of phosphorus biogeochemistry in the rhizosphere. Plant Soil 424, 573–589.
Larsen, M., Borisov, S.M., Grunwald, B., Klimant, I., Glud, R.N., 2011. A simple and inexpensive high resolution color ratiometric planar optode imaging approach: application to oxygen and pH sensing. Limnol. Oceanogr. Methods 9, 348–360.
Lehto, N.J., Davison, W., Zhang, H., 2012. The use of ultra-thin diffusive gradients in thin-films (DGT) devices for the analysis of trace metal dynamics in soils and sediments: a measurement and modelling approach. Environ. Chem. 9, 415–423.
Li, C., Ding, S., Yang, L., Wang, Y., Ren, M., Chen, M., Fan, X., Lichtfouse, E., 2019. Diffusive gradients in thin films: devices, materials and applications. Environ. Chem. Lett. 17, 801–831.
Li, C., Ding, S., Yang, L., Zhu, Q., Chen, M., Tsang, D.C., Cai, G., Feng, C., Wang, Y., Zhang, C., 2019. Planar optode: a two-dimensional imaging technique for studying spatial-temporal dynamics of solutes in sediment and soil. Earth. Rev., 102916
McKenzie, R., 1980. The adsorption of lead and other heavy metals on oxides of manganese and iron. Soil Res. 18, 61–73.
Mishra, S., Bharagava, R.N., More, N., Yadav, A., Zainith, S., Mani, S., Chowdhary, P., 2019. Heavy metal contamination: an alarming threat to environment and human health. Environmental Biotechnology: for Sustainable Future. Springer, pp. 103–125.
Morse, J.W., 1991. Oxidation kinetics of sedimentary pyrite in seawater. Geochim. Cosmochim. Acta 55, 3665–3667.
Moses, C.O., Herman, J.S., 1991. Pyrite oxidation at circumneutral pH. Geochim. Cosmochim. Acta 55, 471–482.
Naylor, C., Davison, W., Motelica-Heino, M., Van Den Berg, G., Van Der Heijdt, L., 2004. Simultaneous release of sulfide with Fe, Mn, Ni and Zn in marine harbour sediment measured using a combined metal/sulfide DGT probe. Sci. Total Environ. 328, 275–286.
Nelson, D.C., Amend, J., Edwards, K., Lyons, T., 2004. Sulfide Oxidation in Marine Sediments: Geochemistry Meets Microbiology, Special Paper 379: Sulfur Biogeochemistry-past and Present, pp. 63–81.
Preisler, A., De Beer, D., Lichtschlag, A., Lavik, G., Boetius, A., Jørgensen, B.B., 2007. Biological and chemical sulfide oxidation in a Beggiatoa inhabited marine sediment. ISME J. 1, 341.
Ratié, G., Vantelon, D., Kalahroodi, E.L., Bihannic, I., Pierson-Wickmann, A.-C., Davranche, M., 2019. Iron speciation at the riverbank surface in wetland and potential impact on the mobility of trace metals. Sci. Total Environ. 651, 443–455.
Sarwar, N., Imran, M., Shaheen, M.R., Ishaque, W., Kamran, M.A., Matloob, A., Rehim, A., Hussain, S., 2017. Phytoremediation strategies for soils contaminated with heavy metals: modifications and future perspectives. Chemosphere 171, 710–721.
Schindler, D.W., Carpenter, S.R., Chapra, S.C., Hecky, R.E., Orihel, D.M., 2016. Reducing phosphorus to curb lake eutrophication is a success, in. ACS Publications.
Stahl, H., Warnken, K.W., Sochaczewski, L., Glud, R.N., Davison, W., Zhang, H., 2012. A combined sensor for simultaneous high resolution 2-D imaging of oxygen and trace metals fluxes. Limnol. Oceanogr. Methods 10, 389–401.
Stockdale, A., Davison, W., Zhang, H., 2008. High-resolution two-dimensional quantitative analysis of phosphorus, vanadium and arsenic, and qualitative analysis of sulfide, in a freshwater sediment. Environ. Chem. 5, 143–149.
Teasdale, P.R., Hayward, S., Davison, W., 1999. In situ, high-resolution measurement of dissolved sulfide using diffusive gradients in thin films with computer-imaging densitometry. Anal. Chem. 71, 2186–2191.
Valentinuzzi, F., Mimmo, T., Cesco, S., Al Mamun, S., Santner, J., Hoefer, C., Oburger, E., Robinson, B., Lehto, N., 2015. The effect of lime on the rhizosphere processes and elemental uptake of white lupin. Environ. Exp. Bot. 118, 85–94.
Wang, Y., Ding, S., Gong, M., Xu, S., Xu, W., Zhang, C., 2016. Diffusion characteristics of agarose hydrogel used in diffusive gradients in thin films for measurements of cations and anions. Anal. Chim. Acta 945, 47–56.
Wang, Y., Ding, S., Ren, M., Li, C., Xu, S., Sun, Q., Xu, L., 2019. Enhanced DGT capability for measurements of multiple types of analytes using synergistic effects among different binding agents. Sci. Total Environ. 657, 446–456.
Warnken, K.W., Zhang, H., Davison, W., 2004. Analysis of polyacrylamide gels for trace metals using diffusive gradients in thin films and laser ablation inductively coupled plasma mass spectrometry. Anal. Chem. 76, 6077–6084.
Weidner, E., Ciesielczyk, F., 2019. Removal of hazardous oxyanions from the environment using metal-oxide-Based materials. Materials 12, 927.
Xu, D., Chen, Y., Ding, S., Sun, Q., Wang, Y., Zhang, C., 2013. Diffusive gradients in thin films technique equipped with a mixed binding gel for simultaneous measurements of dissolved reactive phosphorus and dissolved iron. Environ. Sci. Technol. 47, 10477–10484.
Yabutani, T., Ji, S., Mouri, F., Sawatari, H., Itoh, A., Chiba, K., Haraguchi, H., 1999. Multielement determination of trace elements in coastal seawater by inductively coupled plasma mass spectrometry with aid of chelating resin preconcentration. Bulletin of The Chemical Society of Japan - BULL CHEM SOC JPN 72, 2253–2260.
Zhang, H., Davison, W., 1995. Performance characteristics of diffusion gradients in thin films for the in situ measurement of trace metals in aqueous solution. Anal. Chem. 67, 3391–3400.
Zhou, C., van de Velde, S., Baeyens, W., Gao, Y., 2018. Comparison of Chelex based resins in diffusive gradients in thin-film for high resolution assessment of metals. Talanta 186, 397–405.
Zhu, Q., 2019. In situ planar optical sensors for sediment diagenesis study. in: Encyclopedia of Ocean Sciences 147–156.
Zoroddu, M.A., Aaseth, J., Crisponi, G., Medici, S., Peana, M., Nurchi, V.M., 2019. The essential metals for humans: a brief overview. J. Inorg. Biochem.